Dalton Transactions

PAPER

View Article Online
View Journal | View Issue

CrossMark click for updates

Cite this: *Dalton Trans.*, 2014, **43**, 13545

Computed ligand effects on the oxidative addition of phenyl halides to phosphine supported palladium(0) catalysts†

Claire L. McMullin,§ Natalie Fey* and Jeremy N. Harvey*

Received 13th June 2014,
Accepted 23rd July 2014

DOI: 10.1039/c4dt01758g

www.rsc.org/dalton

The manifold of reaction pathways for the oxidative addition of phenyl bromide and phenyl chloride substrates to phosphine-modified palladium(0) complexes has been investigated with dispersion-corrected density functional theory (B3LYP-D2) for a range of synthetically relevant ligands, permitting the evaluation of ligand, substrate and method effects on calculated predictions. Bulky and electron-rich ligands P^tBu_3 and SPhos can access low-coordinate complexes more easily, facilitating formation of the catalytically active species throughout the cycle. While the bisphosphine oxidative addition step is reasonably facile for the smaller PCy_3 and PPh_3 ligands, the dissociation of these ligands to generate reactive palladium complexes becomes more important and the catalyst is more likely to become trapped in unreactive intermediates. This study demonstrates the feasibility of exploring the catalytic manifold for synthetically relevant ligands with computational chemistry, but also highlights the remaining challenges.

Introduction

Palladium-catalyzed cross-coupling reactions have been developed to accommodate a variety of substrates,[1] permitting the formation of new C–C or C–Y bonds, where Y is a heteroatom. The importance of this group of reactions was internationally recognized in 2010, when the Nobel prize for Chemistry was jointly awarded to Heck,[2] Negishi[3] and Suzuki[4] for their research on C–C bond formation. Other researchers who have also contributed to this field include Kumada,[5] Stille,[6] and Hiyama,[7] as well as Buchwald[8] and Hartwig,[9] who have made significant contributions to a range of carbon–heteroatom bond forming reactions. Computational studies of C–C cross-coupling reactions have recently been reviewed,[10] as have studies combining experimental and computational data to gain insight into palladium catalysis.[11]

A key step of these reactions, in common with some palladium-catalyzed C–H activation reactions,[12] is the oxidative addition of an aryl or alkyl halide to the palladium centre (Scheme 1). The activation of the Pd(0) catalyst, followed by insertion of the metal atom into the C_{ipso} and halide (X) (or triflate, SO_3CF_3) bond, has been shown to be rate limiting in certain conditions.[13]

$$[Pd^0L_n] \xrightarrow{+\ ArX} [Pd^{II}L_n(Ar)(X)]$$

Scheme 1 Oxidative addition step for an aryl halide (ArX) with a palladium(0) catalyst.

Broadly, catalyst design to support oxidative addition can be formulated as requiring an electron rich palladium centre, which supports the increase in oxidation state from Pd(0) to Pd(II).[14] The catalyst also needs to tolerate an increase in coordination number during the oxidative addition by starting out as low-coordinate or through the facile loss of one/several ligands.[15] Furthermore, the system must remain active through multiple cycles, either by avoiding resting states and inactive reservoir species,[16] or by re-entering the catalytic cycle relatively easily.

Ligands are often key to the fine-tuning of the activity and selectivity of organometallic catalysts. In general, electron-donating spectator ligands are favoured for oxidative additions,[17] and steric bulk can be used to support lower coordination numbers for the initial $[PdL_n]$ species; the ligands shown in Scheme 2 fulfill these criteria and patented systems for cross-coupling reactions have been reviewed.[17]

With a view to exploring and enhancing the role computational chemistry can play in the process of ligand-driven catalyst discovery and design we have been pursuing a computational methodology for the analysis and prediction of ligand

School of Chemistry, University of Bristol, Cantock's Close, Bristol, BS8 1TS, UK. E-mail: Natalie.Fey@bristol.ac.uk, Jeremy.Harvey@bristol.ac.uk; Fax: +44 (0)117 9251295

†Electronic supplementary information (ESI) available: Full computational details, further calculation results and detailed breakdown of results for all ligands at all levels of theory, conformer classifications and *xyz* coordinates of all optimised structures. See DOI: 10.1039/c4dt01758g

§Present address: Institute of Chemical Sciences, Heriot-Watt University, Edinburgh, EH14 4AS. E-mail: c.l.mcmullin@hw.ac.uk.

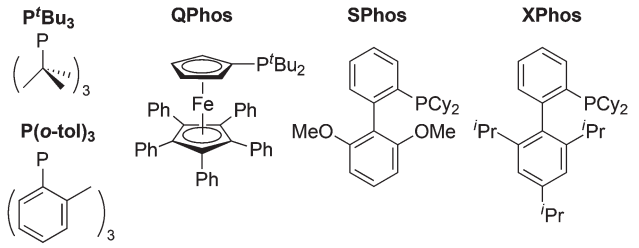

Scheme 2 Popular, experimentally used monodentate phosphine spectator ligands (L) in palladium catalyzed oxidative addition, including P^{t}Bu$_3$,[18] P(*o*-tol)$_3$[19] and QPhos,[20] as well as SPhos and XPhos ligands from the biaryl-alkylphosphine family developed by Buchwald and co-workers.[21]

effects in homogenous organometallic catalysis, combining DFT-calculated ligand property parameters[22] with the analysis and prediction of both experimental[23] and calculated[24] data capturing catalyst performance, such as yield, rates and barriers to reaction. Accurate computational studies of catalytic cycles, especially where a manifold of competing reaction pathways exists, are an important component of this methodology and we have evaluated the impact of computational method effects to establish and validate a theoretical approach suitable for the study of the key oxidative addition step for synthetically relevant organometallic catalysts.[25] In this earlier work, we deliberately focused on the P^{t}Bu$_3$ ligand because its large steric bulk restricts the number of accessible reaction pathways in the mechanistic manifold and limits the number of complexes and conformers which need to be considered.

For other, slightly smaller ligands such as PPh$_3$ and PCy$_3$, a number of additional steps/pathways may become energetically accessible and hence need to be taken into account (Scheme 3), making the study of these ligands computationally more demanding. In order to permit energetic comparison of competing pathways and comparison with experiment, the computational approach used must be sufficiently accurate, which requires it to take account of solvation,[26] dispersion[27] and vibrational corrections.[28]

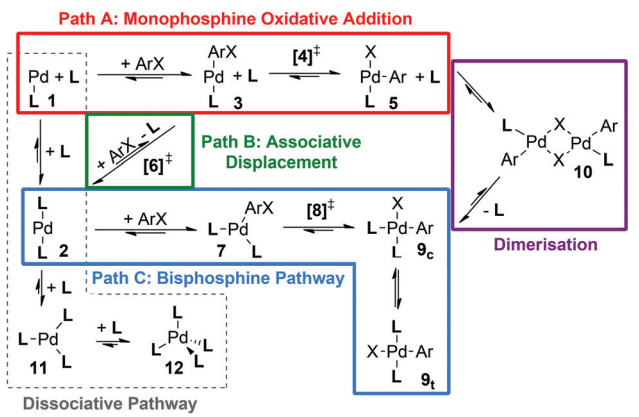

Scheme 3 Reaction pathways and intermediates for the oxidative addition of ArX by a palladium catalyst [PdL$_n$].

The exact energetic balance of such competing pathways will be influenced most profoundly by both the ligand and the aryl/alkyl halide used. Here we report calculated results for the oxidative addition of two aryl halides (PhBr and PhCl) to a palladium centre supported by a number of synthetically useful ligands (PCy$_3$, PPh$_3$, P^{t}Bu$_3$ and the SPhos ligand as a representative of the family of biaryl ligands developed in Buchwald's group[21]). Results for the PCy$_3$ ligand and a phenyl bromide substrate will be used to map out competing dissociative and associative pathways; this ligand has been used experimentally in a range of cross-coupling reactions with less activated aryl chloride and aryl triflate substrates[29] and has been the subject of several experimental kinetic studies,[13a,30] providing experimental data to validate calculated results. Ligand effects on the mechanism have also been considered for additional, synthetically relevant ligands (PPh$_3$, SPhos, P^{t}Bu$_3$) and the interplay between ligand and substrate effects has been evaluated by comparing data for PhBr and PhCl substrates in the presence of these ligands. These results have been used to illustrate what can be achieved with the methodology used, but also to discuss where computational improvements might be made in the future.

Mechanistic manifold

As indicated in Scheme 3, a number of different pathways and species can be envisaged as part of the mechanistic manifold for palladium-catalyzed oxidative addition. Depending on ligand size and donor strength, as well as the catalyst precursor used, the initial coordination number of the palladium(0) species [PdL$_n$] can take values of n = 1–4 (**1**, **2**, **11** or **12**), although the monoligated complex **1** has not been detected experimentally for any ligand in solution;[31] solvent coordination might occur in this case.[13b,31a,32]

For large ligands it has often been assumed that the active species which undergoes oxidative addition is the monophosphine complex [PdL], **1**, formed after ligand dissociation from the bisligated [PdL$_2$] species (**2**),[30a,33] potentially stabilized by solvent coordination.[13b,31a,32] However, the trisligated and tetrakisligated [PdL$_n$] species, **11** and **12** respectively, have been observed experimentally for ligands PCy$_3$ and PPh$_3$,[30a,b,34] and this has recently been confirmed computationally for PPh$_3$,[35] with kinetic studies showing that in solution [PdL$_4$] (**12**) easily loses one or two ligand molecules, to form a rapidly equilibrating mixture of [PdL$_3$] (**11**) and [PdL$_2$] (**2**).[30a,36] [PdL$_2$] (**2**) and [PdL] (**1**) have also recently been observed in the gas phase when L = [PPh$_2$(*m*-C$_6$H$_4$SO$_3$)]$^-$.[31b]

One dissociative pathway and two associative pathways (Scheme 3) could lead to the oxidative addition of an aryl halide to the catalyst. In the *dissociative pathway* (Scheme 3, shown in pale grey outline), ligand loss would occur before coordination of the aryl halide substrate to form the [PdL(ArX)] adduct **3**, and then undergo monoligated oxidative addition *via* [**4**]‡. The dissociative pathway links with monophosphine oxidative addition (Path A, red outline) *via* the [PdL] complex **1**.

In the first associative bisphosphine pathway (Path B), associative displacement of one ligand by the aryl halide substrate *via* [**6**]‡ can generate the [PdL(ArX)] adduct **3**. At this stage the pathway merges with Path A and oxidative addition occurs to the monoligated metal center *via* TS [**4**]‡ (*associative displacement pathway* (Path B, connection to Path A shown in green in Scheme 3)). Alternatively, the metal remains bisligated and the oxidative addition occurs directly to [PdL_2] (**2**) *via* [**8**]‡, possibly *via* a (transient) adduct of the form [PdL_2(ArX)] (**7**); this will be denoted as the *bisphosphine pathway* (Path C, Scheme 3, shown in blue). A further alternative, where solvent is weakly coordinated by [PdL] **1**,[13b,31a,32] has also been considered for L = P^tBu_3 (section ESI2†).

Depending on the pathway followed, a range of different complexes can result from the oxidative addition. Monoligation during the oxidative addition transition state, accessed by pathways A and B, will initially produce three possible isomers of a T-shaped complex, [Pd(L)(Ar)(X)] **5**. The isomer with the phosphine ligand *trans* to the halide has been observed crystallographically for P^tBu_3, whose steric bulk and ability to form γ-agostic interactions with the metal can protect the adjacent vacant coordination site on the metal.[15,37] For smaller ligands, the monoligated product **5** can undergo ligand addition to form square-planar *cis* or *trans* isomers of [PdL_2(Ar)(X)], *c*-**9** or *t*-**9**; both isomers have been observed crystallographically (see, for example, ref. 38 (PPh_3)). The *cis* isomer *c*-**9** can also be reached directly by oxidative addition to a bisligated palladium center (Path C), which may be followed by isomerisation to give *t*-**9**.

Alternatively, **5** can coordinate a second T-shaped complex to form a halide bridged dinuclear complex [$(\mu\text{-X})_2Pd_2(L)_2(Ph)_2$] **10**, which again adopts a square-planar geometry around each metal center for either an *anti* or a *syn* dimer (*a*-**10** and *s*-**10** respectively), observed crystallographically for P^tBu_3 and P(1-Ad)^tBu_2,[13a] as well as P(*o*-tol)$_3$[19a,b] and CataCXiumA.[39] Based on a computational study by Lledós, Espinet and co-workers, albeit without consideration of dispersion corrections, the observed higher activity of bulky ligands may be related to avoiding the formation of side products and reservoir species such as **9** and **10**.[40]

Method effects on prediction

Before describing our results on the different mechanisms and ligands, we first consider how the results depend on the computational protocol, for the case of speciation in solution between the different [$Pd(PCy_3)_n$] complexes (n = 1–3). As in our previous work,[25b] the geometry of all species has been optimized using the B3LYP functional in vacuum, with a medium basis set (denoted as BS1), followed by single-point energy calculations of the dispersion correction¶ and with larger basis sets (BS2) (see computational details below and the ESI†). The effect of geometry optimisation with dispersion-corrected functionals was found to be generally modest, but might make a more important contribution for crowded complexes involved in Path C, see discussion below and in section ESI3.† We have then computed vibrational frequencies and used ideal gas statistical mechanics to compute relative free energies in vacuum. These have been corrected by solvation free energies computed using continuum methods.[41]

We note that some authors have argued that this approach exaggerates entropic effects, which are smaller in solution than in the gas phase.[42] However, such effects should in principle be treated adequately by the continuum model. In our experience, discrepancies with experiment observed when using this approach, instead of being due to such entropic factors, can be the result of inaccurate electronic structure theory. For relative energies, this can arise, for example, from the neglect of dispersion interactions in many density functional theory methods, underestimating the stabilization of higher coordination numbers. We note also that for complex systems such as those considered here, it is essential to identify correctly the lowest-energy isomer and conformer of each of the minima and transition states involved.[43] Finally, while anionic metal complexes have been observed to play a role in Heck and cross-coupling reactions performed in polar solvents and with some palladium precursors ($Pd(OAc)_2$, $Pd(dba)_2$),[44] here we focused on reactions in toluene, where these species are less likely to play a dominant role.[30b] The same applies to mechanisms for oxidative addition of alkyl halides, RX, in which the metal centre attacks the carbon atom to displace X^-, which only subsequently adds to the metal. While there is evidence for such mechanisms with RX and in more polar conditions, they should play little role here.

Table 1a and Fig. 1 show calculated relative free energies of different coordination numbers for the three [$Pd(PCy_3)_n$] species (n = 1–3), at different levels of theory.‖ Experimentally, solutions are found to contain a mixture of the n = 2 and n = 3 species. Measurement of the equilibrium constant at temperatures between −68 and −85 °C yields an experimental enthalpy for binding of L to PdL_2 in solution of about −5 kcal mol^{-1}.[30a] This is not readily comparable to computation as it includes solvent *enthalpic* effects, which are not easily computed using continuum solvent methods. The standard Gibbs energy for binding is negative at lower temperatures, but increases at higher temperatures. Extrapolation of these experimental data suggests a $\Delta G°$ of binding of −0.7 kcal mol^{-1} at 25 °C, and of +0.3 kcal mol^{-1} at 100 °C.

It can be noted that at the B3LYP level of theory, PdL_3 lies *higher* in energy than PdL_2 + L, and much higher in Gibbs energy as ligand dissociation is entropically favourable. This clearly disagrees with the experimental values. This has also been observed for L = PPh_3 by Ahlquist and Norrby.[35]

¶We have used Grimme's "D2" correction here to facilitate comparison with our P^tBu_3 results published previously (ref. 25*b*). We note that the "D3" dispersion correction has since been described (in S. Grimme, J. Antony, S. Ehrlich and H. Krieg, *J. Chem. Phys.*, 2010, **132**, 154104), which Grimme recommends as superior. Our own test calculations (some of which are summarised in Table ESI4f†) suggest that the version of the dispersion correction does not substantially alter the trends and conclusions described here.

‖ In figures and tables, free ligand L needed to achieve stoichiometrically correct notation will frequently be left out, *e.g.* where the Gibbs energy of "[PdL_3]" is compared to that of "[PdL_2]", the calculated number will be based on comparing the calculated Gibbs energy of [PdL_3] to the sum of those for [PdL_2] + L.

Table 1 Favoured metal coordination number for $[PdL_n]$ complexes, L = PCy_3 (all energies are given in units of kcal mol^{-1} and relative to $[PdL_2]$ (**2**)

(a) Method effects at 90 °C

	n	ΔE (BS2)	$\Delta G°$ (BS2)	$\Delta G°$ (BS2) + ΔG_{solv}	ΔE-D (BS2)	$\Delta G°$-D (BS2)	$\Delta G°$-D (BS2) + ΔG_{solv}
$\mathbf{1}_{Cy}$	1	32.9	20.1	8.1	43.4	30.6	18.5
$\mathbf{2}_{Cy}$	2	0.0	0.0	0.0	0.0	0.0	0.0
$\mathbf{11}_{Cy}$	3	10.3	32.3	39.3	−26.3	−4.2	2.7

(b) Temperature effects on favoured coordination number (note that the temperature dependence of the solvent contribution has been neglected here). See ESI for a more detailed breakdown of energy contributions‖

	n	$\Delta G°$-D (90 °C) + ΔG_{solv}	$\Delta G°$-D (10 °C) + ΔG_{solv}	$\Delta G°$-D (−60 °C) + ΔG_{solv}
$\mathbf{1}_{Cy}$	1	18.5	20.9	23.5
$\mathbf{2}_{Cy}$	2	0.0	0.0	0.0
$\mathbf{11}_{Cy}$	3	2.7	−1.5	−5.8

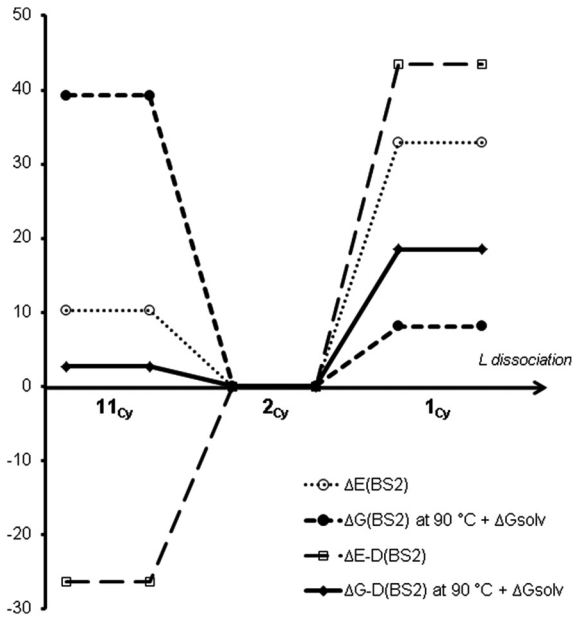

Fig. 1 Method effects on the coordination number of $[PdL_n]$ for L = PCy_3 at 90 °C (all energies are given in kcal mol^{-1} and are calculated relative to $[PdL_2]$, see also Table 1a).

On the other hand, upon including an approximate treatment of dispersion (ΔE-D(BS2)),¶ the $[PdL_3]$ species is found to lie much lower in potential energy compared to $[PdL_2]$ and L in vacuum. The computed *Gibbs energy* of binding is now close to zero, and, in excellent agreement with experiment, is calculated to be small and negative near room temperature. The agreement with experiment is less good at higher and lower temperatures, perhaps because the temperature dependence of the solvation Gibbs energy has been neglected here. The continuum model is parameterized to give accurate results at room temperature and may be less reliable at higher and lower temperatures. Nevertheless, the present tests suggest that our chosen "best" computational protocol yields results within a few kcal mol^{-1} of experiment. In the rest of the paper, only these "best" computed standard free energies will be discussed, with all results corrected for a reaction temperature of 90 °C. A breakdown of energy contributions for each ligand may be found Tables S2–5.†

Ligand effects

Table 2 shows results for ligands discussed here; PCy_3, PPh_3, and SPhos, with previously published[25b] and additional data for P^tBu_3 also included for comparison. Both PCy_3 and SPhos ligands can adopt a number of different conformers and these have been explored by mining of the Cambridge Structural Database (CSD)[45] and DFT calculations in different coordination environments, see section ESI3† for details. All energies shown are given relative to $[PdL_2]$ + PhX and corrected for a reaction temperature of 90 °C, chosen to allow direct comparison with previous work.[25b]

(a) PCy_3. As discussed in the previous section, at our "best" level of theory, the $[Pd(PCy_3)_2]$ complex $\mathbf{2}_{Cy}$ is slightly favoured over the trisligated complex $\mathbf{11}_{Cy}$ at 90 °C, while

Table 2 B3LYP-D2/BS2 Gibbs energies in kcal mol^{-1} for the oxidative addition of PhBr to $[PdL_n]$, see Scheme 3 for details and Tables S2–S5 for detailed energy contributions‖

	$\Delta G°$ (90 °C) + ΔG_{solv}	PCy_3	PPh_3	SPhos	P^tBu_3
1	[PdL] + PhBr	18.5	18.4	2.4	25.7
2	$[PdL_2]$ + PhBr	0.0	0.0	0.0	0.0
3	[PdL(PhBr)]	14.0	14.4	11.0	18.6
[**4**]‡	[PdL(Ph···Br)]‡	22.7	24.7	19.6	26.9
5	[PdL(Ph)(Br)]	−9.3	−6.4	−19.5	−1.2
[**6**]‡	$[PdL_2(PhBr)]^‡$	28.6	24.9	29.1	29.2
7	$[PdL_2(PhBr)]$	[a]	[a]	[b]	[a]
[**8**]‡	$[PdL_2(Ph···Br)]^‡$	20.6	21.8	[b]	[b]
c-**9**	$[PdL_2(Ph)(Br)]$	[b]	−13.7	[b]	[b]
t-**9**	$[PdL_2(Ph)(Br)]$	−27.3	−19.8	[b]	10.0
a-**10**	$\frac{1}{2}[(\mu\text{-Br})_2Pd_2L_2(Ph)_2]$	−14.1	−13.2	[b]	1.3
s-**10**	$\frac{1}{2}[(\mu\text{-Br})_2Pd_2L_2(Ph)_2]$	[b]	[b]	−19.9	1.0
11	$[PdL_3]$ + PhBr	2.7	−1.9	[b]	[b]
12	$[PdL_4]$ + PhBr	[b]	23.5	[b]	[b]

[a] Optimisation unsuccessful. [b] Not attempted for this ligand.

trisligation becomes more favourable at lower temperatures (see also Table 1b). Attempts to optimize a *tetrakis* [PdL_4] complex for this ligand were unsuccessful and led to ligand dissociation.

Dissociative pathway (A). These results suggest that ligand dissociation to form the low-coordinate [PdL] complex $\mathbf{1_{Cy}}$ is energetically accessible (Fig. 2, labeled in grey, Tables 2 and S2†). This might exist as a transient species or as a solvated intermediate with a solvent molecule coordinated to the palladium centre.[13b,30c,31a] Note that the inclusion of continuum-based solvation free energies in our "best" computed energies should implicitly describe such solvent binding, at least roughly. We have argued previously[25b] that the continuum solvent method may slightly overestimate the solvent stabilization of this highly unsaturated metal centre. In contrast, several computational studies of other ligands have assumed that the active catalyst is the monophosphine complex **1**, formed after ligand dissociation from bisligated [PdL_2], **2**.[10a,33a,b,d,46]

In addition to the dissociated complex $\mathbf{1_{Cy}}$ shown, there will be a point of maximum Gibbs energy along the reaction path for addition of a ligand, or of the aryl halide, to [PdL]. There is no *potential energy* barrier to such additions, with the Gibbs energy barrier being due to loss of entropy upon approach. As in our previous work,[25b] we estimate the Gibbs energy barrier to addition to be *ca.* 4.5 kcal mol^{-1} at 90 °C, based on the rate constants for reactions known to be diffusion-controlled. With this estimate, the transition state (TS) for oxidative addition to the monoligated metal centre $[\mathbf{4_{Cy}}]^{‡}$ is predicted to be very slightly lower in Gibbs energy (at 22.7 kcal mol^{-1}) than the TSs for ligand loss from PdL_2 or for aryl halide addition to PdL (both at *ca.* 23.0 kcal mol^{-1}). However, these values are very close, preventing calculations from distinguishing reliably between these options.

Associative displacement pathway (B). The highest Gibbs energy transition state on this pathway (B, Fig. 2) is for associative displacement of one PCy_3 ligand by the PhBr substrate ($[\mathbf{6_{Cy}}]^{‡}$, 28.6 kcal mol^{-1}), which has the highest barrier of all the pathways considered here, presumably due to considerable ligand steric hindrance. This is one of the two mechanisms that are consistent with the experimentally observed order of reaction in Hartwig's kinetic study.[13a] It is also the mechanism predicted to be favoured with L = P^tBu_3.[25b] However, for PCy_3 it can be discounted based on the present calculations, since the barrier is so much higher than for Path C; this is also consistent with experiment as discussed below.

Bisphosphine pathway (C). The bisligated oxidative addition, $[\mathbf{8_{Cy}}]^{‡}$ (shown as the blue pathway in Fig. 2) has the lowest calculated barrier (20.6 kcal mol^{-1}) of the competing transition states, $[\mathbf{4_{Cy}}]^{‡}$, $[\mathbf{6_{Cy}}]^{‡}$ and $[\mathbf{8_{Cy}}]^{‡}$ studied here. This is in agreement with Hartwig's interpretation of the experimental kinetics,[13a] whereby the irreversible step during the oxidative addition involves a bisligated complex. It is to be noted, though, that this observation is not enough to exclude the associative displacement mechanism discussed above.

Mitchell and Baird carried out careful kinetics studies on the reaction of $Pd(PCy_3)_2$ with PhBr, both in the absence and presence of additional PCy_3, at room temperature.[30b] Added PCy_3 inhibits oxidative addition, decreasing the relative amounts of [$Pd(PCy_3)$] ($\mathbf{1_{Cy}}$) and [$Pd(PCy_3)_2$] ($\mathbf{2_{Cy}}$) due to formation of [$Pd(PCy_3)_3$] ($\mathbf{11_{Cy}}$).[30b] In the absence of additional ligand, the Pd(0) is mostly present in the bisligated form. This is observed to disappear, with a pseudo-first order rate law, with an apparent rate constant given by k[PhBr] + k'. The first term here can be accounted for by the bisphosphine pathway (C). The value of k in their experiments is 1.3 × 10^{-3} M^{-1} s^{-1}, corresponding to a Gibbs energy of activation of 21.3 kcal mol^{-1}. This compares very well to our calculated Gibbs energy of activation (22.8 kcal mol^{-1} at 10 °C, see Table S2b†). The second term can be accounted for by the dissociative pathway (A), with phosphine loss assumed to be rate-limiting, given the low concentration of free L and high concentration of PhBr in these experiments. The value of k' measured, 6.1 × 10^{-4} s^{-1}, would correspond to a Gibbs energy of activation of 21.7 kcal mol^{-1}. Again, this matches our calculated barriers reasonably well (*ca.* 24.5 kcal mol^{-1} at 10 °C from energy for $\mathbf{1_{Cy}}$ + Gibbs energy barrier to ligand addition estimated as detailed above). In experiments carried out in the presence of excess PCy_3, the results suggest that the contribution from the monoligated Path A is suppressed, but the analysis is complicated due to the fact that some of the Pd(0) is now present as PdL_3 which is unlikely to participate in the reaction.

Hartwig *et al.* have also studied the kinetics for this reaction, at the slightly lower temperature of 10 °C, and with an excess of ligand present. They observe a slight decrease in reactivity as more L is added, due to slight changes in the position of the equilibrium with unreactive PdL_3. Reactivity is first-order with respect to [PhBr], and, neglecting the complications

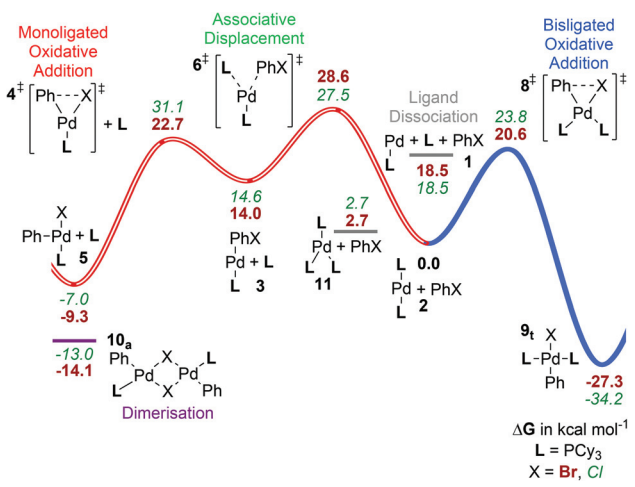

Fig. 2 Gibbs energy surface (Δ*G*° (90 °C) + ΔG_{solv}) for the oxidative addition of PhBr to a [$Pd(PCy_3)_n$] catalyst. All energies are in units of kcal mol^{-1} and relative to [PdL_2]. The blue pathway shown corresponds to the bisligated oxidative addition (C, see Scheme 3), while the red pathway (hollow line) shows the associative displacement route (B), which merges with the dissociative pathway (A) at complex **3** (Scheme 3).

arising from equilibrium with PdL_3, their observed reactivity corresponds to a rate constant of 3×10^{-4} M^{-1} s^{-1}, or to a $\Delta G^{\ddagger}$ of 21 kcal mol^{-1}.** This is consistent with the other experiments, and with our computational results predicting the bisphosphine pathway (C) to be most favourable. The considerable sensitivity to method effects discussed earlier makes it difficult to distinguish confidently between paths A and C based on computation alone, and both pathways could indeed in principle be operating to some extent, though the bisligated path C is more consistent with experiment.

Computational work by Schoenebeck and Houk[29b] has shown that, while calculations suggest the monoligated pathway (A) to be favoured in terms of Gibbs energies, experimentally observed selectivities can only be explained by considering a bisligated oxidative addition pathway (Table S6† gives an overview of the computational approaches used in computational studies referred to). An earlier study involving the sterically and electronically similar[47] P^iPr_3 ligand that included solvation corrections, but not dispersion effects, had also ruled out the bisligated oxidative addition (C), as well as associative displacement (path B), as too high in terms of Gibbs energy.[33a] The discussion of method effects above helps to explain these discrepancies, with the neglect of dispersion effects artificially favouring the dissociative pathway (A).

Products of oxidative addition. The free energies of a range of monoligated and bisligated oxidative addition products are given in Table 2 (complexes **5**, **9**, **10**). Isomer interconversion has been shown by Maseras to be facile for three- and five-coordinate PH_3 complexes, which can be accessed by square-planar complexes if a ligand is dissociated in the former case or ligand/solvent is coordinated in the latter.[42a] Therefore, we have assumed here that interconversion can take place easily to reach the isomer of lowest Gibbs energy. In line with experimental results, where the *trans* complex of $\mathbf{9_{Cy}}$ has been observed as the only product of the oxidative addition,[15,30b] this complex is the only one which could be optimised for the PCy_3 ligand.

(b) PPh_3. Although triphenylphosphine has largely been displaced from widespread experimental use by bulky alkylphosphines†† and biaryl phosphine ligands (Fig. 1 shows some examples, including key references), this ligand can give rise to reasonably useful catalysts for some cross-coupling reactions.[48] In addition, the ligand continues to be a computational benchmark for exploring ligand effects in oxidative addition and cross-coupling reactions.[16,31,33a,d,35,40,43a,49] Fig. 3 summarises the calculation results for oxidative addition (see also Tables 2 and S3†).

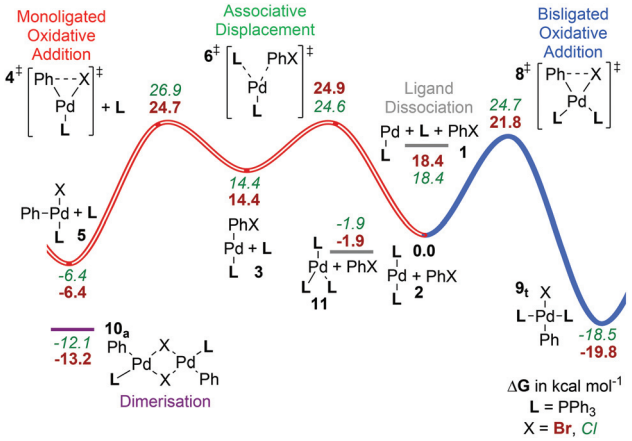

Fig. 3 Gibbs energy surface ($\Delta G°$ (90 °C) + ΔG_{solv}) for the oxidative addition of PhBr to a $[Pd(PPh_3)_n]$ catalyst. See caption of Fig. 2 for labelling conventions used.

Complex $\mathbf{12_{Ph}}$, the *tetrakis* triphenylphosphine palladium(0) complex, has been crystallographically characterized[34b] and is a commercially available precursor for PPh_3-ligated catalysts. In solution, ligand dissociation to the $[PdL_2]$ species $\mathbf{11_{Ph}}$ is known to be near quantitative except at very low temperatures and in the presence of excess phosphine.[36,50] Hence, the equilibrium with $\mathbf{12_{Ph}}$, while it can be observed by ^{31}P-NMR at low temperatures,[50] is not relevant here. Dissociation of $\mathbf{11_{Ph}}$ to form bisligated $\mathbf{2_{Ph}}$ is found experimentally to be unfavourable, with a dissociation equilibrium constant of the order of 10^{-4} M.[34a] Our calculations underestimate the stability of $\mathbf{12_{Ph}}$ significantly: this species is predicted to be much higher in Gibbs energy than $\mathbf{11_{Ph}}$ + L. This is probably an artifact associated with carrying out geometry optimization at a level of theory that does not account for dispersion. Indeed, test optimisations with B3LYP-D2 (section ESI4†) show a significant change in geometry. This is also in agreement with previous work,[27,35] showing reasonable stability for $\mathbf{12_{Ph}}$ when using methods that account for dispersion in optimization as well as energy calculations; for a more general overview, see *e.g.* a recent study by Jensen *et al.*[51]

It appears that this shortcoming in our calculations mainly affects the very crowded complexes, such as $\mathbf{12_{Ph}}$; see the ESI† for a more complete discussion. The calculated ligand binding Gibbs energy required to transform $\mathbf{11_{Ph}}$ into $\mathbf{2_{Ph}}$ is 2.9 kcal mol^{-1} at 25 °C, corresponding to a dissociation equilibrium constant of 8×10^{-3}. The experimental estimate for this dissociation constant places it as being significantly smaller than 10^{-4} M.[34a]

Considering the three possible oxidative pathways starting from the $[PdL_2]$, $\mathbf{2_{Ph}}$, complex, as with PCy_3 our calculations predict that the *bisphosphine pathway* C is favoured, proceeding *via* $[\mathbf{8_{Ph}}]^{\ddagger}$, with a barrier of 21.8 kcal mol^{-1} *vs.* $\mathbf{2_{Ph}}$, and a barrier of 23.7 kcal mol^{-1} *vs.* $\mathbf{11_{Ph}}$ (90 °C, blue pathway in

** They also studied the reaction with PhI, in the presence of excess L and at the low temperature of −80 °C. Under these conditions, the Pd will be present predominantly as PdL_3, and accordingly inverse first-order kinetics with respect to L are observed. The free energy of dissociation of L at this temperature is 2.3 kcal mol^{-1}.[30a] The observed rate-constant obtained by Hartwig *et al.*,[13a] is 8.5 $\times 10^{-4}$ M^{-1} s^{-1}, corresponding to a $\Delta G^{\ddagger}$ of 13.8 kcal mol^{-1}. This would correspond to a $\Delta G^{\ddagger}$ with respect to PdL_2 of 11.5 kcal mol^{-1}, which is lower than calculated here for PhBr – as expected for the more reactive iodide.

†† Different steric measures can be considered, *e.g.* PPh_3 has a Tolman cone angle[66] of 145° and a He_8 steric parameter[47] of 8.0 kcal mol^{-1}, whereas the corresponding data for PCy_3 are 170°, and 15.5 kcal mol^{-1} respectively. Both sets of data indicate that PCy_3 is larger.

Fig. 3) to be favoured. The competing associative displacement route (B, red in Fig. 3) has a highest barrier ($[\mathbf{6_{Ph}}]^{‡}$) of 24.9 kcal mol^{-1} above $\mathbf{2_{Ph}}$, and the highest point of the monoligated oxidative addition pathway ($[\mathbf{4_{Ph}}]^{‡}$) lies 24.7 kcal mol^{-1} above reactants. The *trans*-bisligated product complex (*t*-**9**) is predicted to be most stable for this ligand and has indeed been observed crystallographically.[38b]

The bisphosphine pathway (C) was also found to be favoured by Kozuch and Martin.[16] An earlier study by Fu, Liu *et al*. compared the three different pathways, but, in the absence of dispersion corrections, found both paths B and C to involve much higher Gibbs energy barriers than path A, in line with the analysis of method effects detailed above.[33a]

Experimentally, kinetic data for oxidative addition of various aryl halides to solutions of $\mathbf{12_{Ph}}$ is available for comparison.[30c,34a,52] For the case of PhBr, an apparent rate constant k_{app} = 9 × 10^{-4} M^{-1} s^{-1} was measured at 25 °C for reaction with $\mathbf{12_{Ph}}$.[30c] In fact, under the conditions used, $\mathbf{12_{Ph}}$ will have fully dissociated to $\mathbf{11_{Ph}}$, which will itself be in equilibrium with a small amount of $\mathbf{2_{Ph}}$. Assuming that the latter reacts with PhBr with a rate constant *k*, then $\mathbf{11_{Ph}}$ will decay with $k_{app} = kK/[PPh_3]$. Given that $[PPh_3]$ was equal to 0.002 M in the experiments, this means that *kK* equals 1.8 × 10^{-6} s^{-1}, equivalent to an activation Gibbs energy of 25.2 kcal mol^{-1}, in reasonable agreement with the value of 24.0 kcal mol^{-1} at 25 °C calculated for pathway C here.

(c) SPhos. Developed in the late 1990s,[53] palladium ligated complexes of SPhos, $PCy_2(C_6H_4\text{-}2,6\text{-}(OMe)_2\text{-}C_6H_3)$ (Fig. 1), enhance reactivity for very hindered substrates in Suzuki cross-coupling reactions,[21a] and in particular for aryl chlorides,[54] at low catalyst loadings. The design of these dialkylbiarylphosphines was aimed at stabilizing the oxidative addition intermediate by using bulky and electron-donating phosphines.[54,55] However, it became apparent that palladium complexes can exhibit interactions between Pd and the second ring of the biaryl group which extend the catalyst's lifetime,[21a] preventing cyclometallation and the formation of palladacycles. The steric bulk of alkyl substituents and additional groups on the biaryl unit also serves to increase the stability and concentration of the monoligated Pd(L) species (**1**), considered key in the oxidative addition of aryl chlorides.[21a]

Computational modelling of this ligand is challenging, as both the cyclohexyl and biaryl substituents can adopt a range of conformations and their motion is likely to be correlated. We have found that the nature of the preferred conformer changes for the different species involved in oxidative addition, as shown in Table 3. As discussed in ESI3,† both biaryl and cyclohexyl group orientations respond to the coordination environment and these have been sampled extensively. While the effect of biaryl rotation has been explored previously,[56] consideration of cyclohexyl conformational preferences was less complete and our present work has used a more extensive approach, combining database mining of the CSD[45] and DFT calculations to identify the lowest energy conformer for each complex (section ESI3†). Table 2 and Fig. 4 show results for the conformer compatible with all steps, assuming

Table 3 Relative Gibbs energies ($\Delta G°$ at 90 °C + ΔG_{solv}) in kcal mol^{-1} for different conformations of SPhos, [Pd(SPhos)] and [Pd(SPhos)$_2$]. Energies are given relative to the *lowest* conformer found for each complex

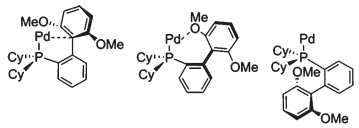

$\mathbf{S_a}$ Pd···C$_\pi$ arene interaction | $\mathbf{S_b}$ Pd···O interaction | $\mathbf{S_c}$ no interaction

		$\mathbf{S_a}$	$\mathbf{S_b}$	$\mathbf{S_c}$
	SPhos	0.0	—[a]	4.3
$\mathbf{1_{SP}}$	[Pd(SPhos)]	9.7	—	0.0
$\mathbf{2_{SP}}$	[Pd(SPhos)$_2$]	0.3 ($\mathbf{S_{ac}}$)[b]	0.0 ($\mathbf{S_{ab}}$)	7.4 ($\mathbf{S_{cc}}$)[c]

[a] Optimises to $\mathbf{S_a}$. [b] Geometry taken from crystal structure [Pd(SPhos)$_2$], CSD ref. MAKBIK.[54] [c] Geometry taken from crystal structure *trans*-[PdCl$_2$(SPhos)$_2$], CSD ref. MAKBEG.[54]

that barriers to conformational change are lower in Gibbs energy than 'reactive' barriers lying along the oxidative addition mechanistic route.

Low coordination numbers for this ligand are stabilized by the biaryl group coming into close proximity to the palladium centre,[56] either providing sites for secondary interactions with the π-system ($\mathbf{S_a}$) or the oxygens of the methoxy groups ($\mathbf{S_b}$), as well as hampering the coordination of solvent/ligand/substrate through steric bulk. This is discussed in section ESI3.†

For SPhos the *dissociative pathway* (A, $[\mathbf{4_{SP}}]^{‡}$, barrier = 19.6 kcal mol^{-1}) presents the lowest barrier, while the *associative displacement pathway* (B, $[\mathbf{6_{SP}}]^{‡}$) is significantly higher in Gibbs energy. We have not considered the *bisligated pathway* (path C) due to the steric hindrance exerted by two SPhos ligands in *cis* coordination sites. The overall calculated Gibbs energy of activation with this ligand is lower than with the other ligands covered in this study, accounting in part for the success of this ligand in catalysis. To the best of our knowledge, no detailed kinetic studies have been reported for this ligand, preventing further validation against experimental data.

The bromide bridged dimer is quite similar in energy to the monoligated T-shaped product, and indeed a chloride-bridged dimer of SPhos has been isolated and characterized crystallographically.[57] This presumably also contributes to the synthetic utility of the ligand, by minimising the amount of metal complexes present as unreactive reservoir species under catalytic conditions.

(d) P^{t}Bu$_3$. The effect of this ligand on the oxidative addition step has been widely studied, both experimentally[13a,c,15,30a,58] and computationally.[16,29b,32b,33a,40,46,49,59] Our earlier study of oxidative addition[25b] considered only this ligand and showed that computed activation parameters for the two monoligated mechanisms (pathways A and B) could account for the experimentally observed kinetics in a near-quantitative way. We found that it is important to account correctly for both Gibbs energy effects and dispersion interactions

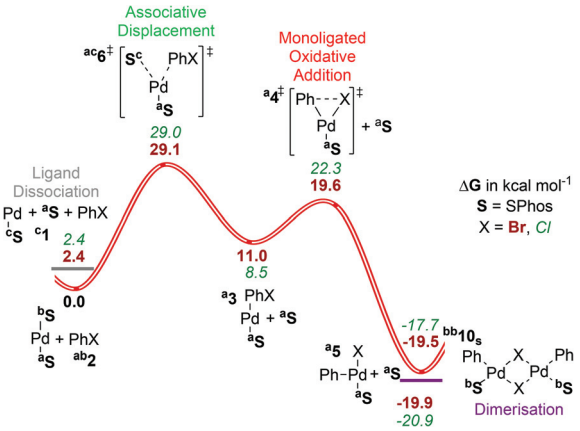

Fig. 4 Gibbs energy surface (Δ*G* (90 °C) + ΔG_{solv}) for the oxidative addition of PhBr to a [Pd(SPhos)$_n$] catalyst. See caption of Fig. 2 for labelling conventions used.

– contrary to many earlier studies that focused on energies and used the B3LYP functional, which does not describe dispersion.[16,25b] Here we report additional results relating to dimer formation to give $\mathbf{10}_{t\mathbf{Bu}}$[40] and the likely stability of a *trans* square planar product complex *t*-$\mathbf{9}_{t\mathbf{Bu}}$, as shown in Table 2. We have also considered associative displacement of one ligand by solvent for this system and these results are included, along with barriers to isomerisation of the T-shaped product $\mathbf{5}_{t\mathbf{Bu}}$ and the intermediate adduct $\mathbf{3}_{t\mathbf{Bu}}$, in section ESI4.† Calculation results have been summarized in Fig. 5 to allow comparison with data for other ligands.

For this ligand, the complex $\mathbf{2}_{t\mathbf{Bu}}$ [Pd(P^{t}Bu$_3$)$_2$] has been characterized crystallographically[60] and no higher coordination numbers have been observed by NMR.[30a] In addition, both the T-shaped oxidative addition product $\mathbf{5}_{t\mathbf{Bu}}$[15] and a chloride bridged-analogue of **10** with an *ortho*-substituted aryl group[13a] have been isolated and characterized crystallographically. The three-coordinate product $\mathbf{5}_{t\mathbf{Bu}}$ is stabilized by agostic interactions between the ligand and the palladium center,[15,61] which reduce the likelihood of dimerisation to form $\mathbf{10}_{t\mathbf{Bu}}$,[21c]

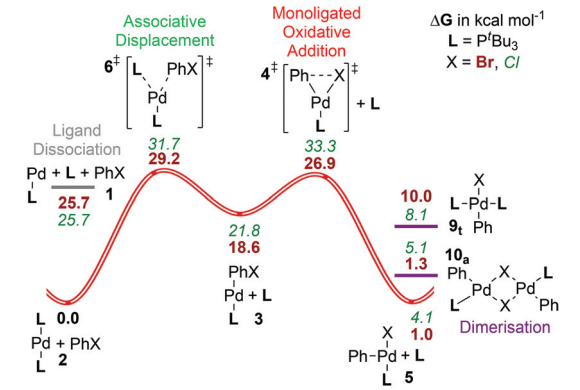

Fig. 5 Gibbs energy surface (Δ*G*° (90 °C) + ΔG_{solv}) for the oxidative addition of PhBr to a [Pd(P^{t}Bu$_3$)$_n$] catalyst. See caption of Fig. 2 for labelling conventions used.

although the results here suggest that this may be finely balanced energetically, with $\mathbf{5}_{t\mathbf{Bu}}$ and both isomers of $\mathbf{10}_{t\mathbf{Bu}}$ lying within less than 2.5 kcal mol^{-1} of each other. Slight modifications of the ligand or the substrate might thus lead to dimerisation and could trap some of the palladium in an unproductive pathway. The *trans* square-planar complex *t*-$\mathbf{9}_{t\mathbf{Bu}}$ lies higher in energy (10.0 kcal mol^{-1}) than the other possible product species.

As we have reported previously,[25b] mechanistically, this ligand presents fewer pathways for evaluation, as the *bisphosphine pathway* (C) is not accessible due to the considerable steric hindrance of two P^{t}Bu$_3$ ligands, which would hamper their *cis* coordination. The preferred mechanism with PhBr involves passing over the *associative displacement* TS (path B) followed by oxidative addition. The key TS lies higher in Gibbs energy ($[\mathbf{6}_{t\mathbf{Bu}}]^‡$, barrier = 29.2 kcal mol^{-1}) than the monoligated oxidative addition (path A, $[\mathbf{4}_{t\mathbf{Bu}}]^‡$, barrier = 26.9 kcal mol^{-1}). Our best estimate places formation of PdL at a Gibbs energy of around 30 kcal mol^{-1},[25b] which, with the variational TSs for addition of L or PhBr, means that path B, *i.e.* the associative displacement route, should be favoured over a dissociative pathway (A) for this ligand. The calculated barrier to associative displacement is in reasonable agreement with available experimental data (see ref. 25*b* for a more detailed discussion).

Before considering substrate effects in greater detail, we can take stock of ligand effects on the likely pathway and energetics of oxidative addition. The calculations reported here, validated where possible by comparison with available experimental data, suggest that very bulky ligands (P^{t}Bu$_3$ and SPhos) favour low-coordinate pathways (A and B). Also, with these ligands, the T-shaped three-coordinate oxidative addition products are reasonably stable towards formation of dimer or bisligated complexes. This is presumably favourable for the reactions following on from oxidative addition in typical catalytic cycles. Smaller ligands, which are less "privileged" in experimental usage, can support higher coordination numbers around the metal centre. This means that prior to oxidative addition, ligand dissociation must occur. Nevertheless, contrary to the more bulky ligands where the C–X bond cleavage event occurs with only a single phosphine coordinated to the palladium centre, for PCy$_3$ and PPh$_3$, the bisphosphine pathway (C) is predicted to dominate. Though the barriers to oxidative addition are similar to or indeed lower than those calculated for bulkier ligands, unproductive product complexes are energetically much more accessible after this step, suggesting that the rate-limiting step for cross-coupling reactions might occur later in the catalytic cycle. Our calculated barriers are generally in good agreement with experimental data where this is available, although we note that detailed kinetic studies of oxidative addition are rare.

Halide effects

The cost of reagents for a chemical reaction can be an important factor, especially when considering the adoption of a new catalytic route. For oxidative addition, this can impact the choice of halide substrate used. Ideally, ligand design can

enable the use of cheaper and structurally more versatile aryl chlorides as substrates.[62] The geometries optimized with phenyl bromide provided a convenient starting point for expanding this study of ligand effects to also consider phenyl chloride as the substrate. "Best method" Gibbs energies for 90 °C to allow comparison with the bromide results are shown in Table 4, with a more detailed breakdown of method effects on energies for all ligands included in Tables S7–S10.†

Experimental and computational studies suggest that the rate limiting step for phenyl chloride oxidative addition is the monophosphine transition state [**4**]‡ (accessed by paths A and B), with limited ligand effects on the likely mechanism for the systems considered.[10a,13a] In Hartwig's experimental kinetic study exploring both ligand and substrate effects,[13a] different rate limiting steps were assigned for the different phenyl halides, with each rate law first order with respect to the concentration of [PdL_2] species (**2**). Chloride substrates showed a dependence on the concentration of the ligand as well as the aryl chloride, thereby indicating that dissociation of a ligand must occur prior to rate-limiting ArCl oxidative addition ([**4**]‡); this transition state contributes to both the dissociative pathway (A) and the associative displacement pathway (B) considered here. As discussed above, the trisligated complex **11** is unlikely to contribute to experimental observations at higher temperature.

Comparison of the *chloro* species (Table 4) with the equivalent *bromo* complexes (Table 2) show that the former have higher relative free energies for transition states, and to some extent also for intermediates, relative to the bisligated reference complex, **2**. The most pronounced substrate effects can be seen for the monophosphine and bisphosphine oxidative addition transition states, [**4**]‡ and [**8**]‡ respectively, as for these barriers different C–halide bonds are broken. For the monoligated oxidative addition, the increase in the barrier ranges from 2.2–8.4 kcal mol^{-1}, with the largest difference observed for [$\mathbf{4_{Cy}}$]‡, whilst for the *bisligated pathway* (C) both PPh_3 and PCy_3 see barrier increases of 2.9 and 3.0 kcal mol^{-1} respectively. The lower reactivity of aryl chlorides has been attributed to the strength of the C–Cl bond,[29a] compared to weaker C–Br and C–I bonds.

Our previous work[25b] showed that for a P^tBu_3 catalyst the change in rate limiting step is observed for the *associative displacement step* (path B), with the *bromo* system limited by the associative displacement of PhBr and a ligand ([$^{Br}\mathbf{6_{tBu}}$]‡), whilst the *chloro* system was restricted by the monophosphine oxidative addition of PhCl ([$^{Cl}\mathbf{4_{tBu}}$]‡), part of paths A and B. For this ligand, dimerisation of the product becomes slightly less likely with the smaller chloride.

With additional results in hand, we can now consider the interplay between ligands and substrates more fully: In the case of PPh_3 no change in favoured mechanism or rate limiting step is predicted by the calculations, although higher barriers suggest a slower rate of reaction, as expected for the chlorides. Similarly, for SPhos, there is no change for the different halide substrates, with the dissociative pathway (A) most likely.

Experimental data is available for the PCy_3 and PCy^tBu_2 cases, from two separate studies. For PCy^tBu_2, the experiments (in toluene at 100 °C) yield rates that vary linearly with substrate concentration, and inversely with concentration of excess ligand. This suggests that path A or B is followed, with insertion into the C–Cl bond rate-limiting. The measured rate constant suggests an activation Gibbs energy of 29.3 kcal mol^{-1}. We have not considered PCy^tBu_2 computationally, but, as in our previous work,[25b] suggest that the calculated properties for P^tBu_3 should be rather similar. As seen in Table 4, our calculations agree well with experiment, showing [**4**]‡ as rate-limiting, and with a relative Gibbs energy of 30.7 kcal mol^{-1}.

For PCy_3, there is the complication that the PdL_2/PdL_3 equilibrium affects observed kinetics (as discussed in the section on method effects above). However, the available experimental data were obtained at fairly low concentration of free L, so that mostly PdL_2 should be present, and we will not consider this equilibrium here. In the study by Hartwig *et al.*,[13a] the measured rates again vary in proportion to substrate concentration, and inversely to concentration of free ligand. This again supports mechanism A or B, with rate limiting oxidative addition through [**4**]‡; the measured rate constant at 70 °C, $k = 1.07 \times 10^{-6}$ s^{-1}, yields a $\Delta G^{\ddagger}$ = 29.4 kcal mol^{-1}. In another experimental study,[30c] the data appear to have been analysed using a rate law that assumes no dependence on concentration of free ligand, and without added ligand. The proposed rate constant of 0.015 M^{-1} s^{-1} at room temperature is at first sight much larger than that reported by Hartwig *et al.*,[13a] but considering the likely very low concentration of free ligand in this study, there is probably no inconsistency. We thus focus our comparison with computation on the results of Hartwig *et al.*[13a] As for P^tBu_3, our calculated transition state ([$^{Cl}\mathbf{4_{Cy}}$]‡) is found to lie at a relative Gibbs energy (31.1 kcal mol^{-1}) that is consistent with experiment. However, our calculations show a significantly lower relative Gibbs energy for the bisligated tran-

Table 4 B3LYP-D2/BS2 Gibbs energies in kcal mol^{-1} for the oxidative addition of PhCl to [PdL_n], see Scheme 3 for details and Tables S7–S10 for detailed energy contributions‖

	$\Delta G°$ (90 °C) + ΔG_{solv}	PCy_3	PPh_3	SPhos	P^tBu_3
1	[PdL] + PhCl	18.5	18.4	2.4	25.7
2	[PdL_2] + PhCl	0.0	0.0	0.0	0.0
3	[PdL(PhCl)]	14.6	14.4	8.5	21.8
[**4**]‡	[PdL(Ph···Cl)]‡	31.1	26.9	22.3	33.3
5	[PdL(Ph)(Cl)]	−7.0	−6.4	−17.7	4.1
[**6**]‡	[PdL_2(PhCl)]‡	27.5	24.6	29.0	31.7
7	[PdL_2(PhCl)]	[a]	[a]	[a]	[a]
[**8**]‡	[PdL_2(Ph···Cl)]‡	23.8	24.7	[b]	[b]
c-**9**	[PdL_2(Ph)(Cl)]	[b]	−13.8	[b]	[a]
t-**9**	[PdL_2(Ph)(Cl)]	−34.2	−18.5	[b]	8.1
a-**10**	$\frac{1}{2}$[(μ-Cl)$_2$Pd$_2$L$_2$(Ph)$_2$]	−13.0	−12.1	[b]	5.1
s-**10**	$\frac{1}{2}$[(μ-Cl)$_2$Pd$_2$L$_2$(Ph)$_2$]	[b]	[b]	−20.9[c]	[b]
11	[PdL_3] + PhCl	2.7	−1.9	[b]	[b]
12	[PdL_4] + PhCl	[b]	21.1	[b]	[b]

[a] Optimisation unsuccessful. [b] Not attempted for this ligand. [c] Looser convergence criteria used for BS2 single point calculation.

sition state ([$^{Cl}\mathbf{8}_{Cy}$]‡), suggesting that path C should instead be favoured. This mechanism is not compatible with the observed kinetics, so it appears that the computational protocol used is not sufficiently accurate for this particular ligand/substrate combination, for reasons that are not yet entirely clear. There are of course many possible sources of inaccuracy – basis set, functional, treatment of dispersion, statistical mechanics for entropy correction, and solvent treatment; some of these effects have been explored in greater detail (see ESI4b–d†). As stated earlier, these effects seem to combine to yield errors of a few kcal mol^{-1} in most cases, but the present case is more sensitive.

Conclusions

The manifold of reaction pathways for the oxidative addition of phenyl halide substrates to phosphine-modified palladium(II) complexes has been investigated with dispersion-corrected density functional theory for a range of synthetically relevant ligands. Three mechanistic possibilities were considered (Scheme 3): (A) a dissociative pathway accessing a low-coordinate [PdL] complex **1**, which undergoes oxidative addition; (B) concerted associative displacement to [PdL_2] **2**, followed by monoligated oxidative addition; (C) a bisligated pathway, where oxidative addition occurs directly to the [PdL_2] complex **2**. Depending on ligand concentration, aryl halide substrate, solvent and temperature, different pathways can be accessed and in some cases, equilibria and competing pathways may need to be considered. Detailed experimental kinetic analysis can supply mechanistic insights and rate constants/barriers in these cases, and here we have been able to use such data to test and validate our computational methodology.

On the whole, the calculated barriers and favoured pathways agree well with the available experimental data, allowing the computational prediction of likely reaction pathway (and hence a rate law), as well as the quantitative analysis of intermediates and transition states.‡‡ In line with ligand design criteria derived from experimental studies, the bulky and electron-rich ligands P^{t}Bu$_3$ and SPhos can access low-coordinate complexes, the most catalytically active species, easily throughout the cycle. While the bisphosphine oxidative addition step is reasonably facile for the smaller PCy_3 and PPh_3 ligands, ligand dissociation to access reactive palladium complexes becomes more important and the catalyst is more likely to become trapped in unreactive intermediates.

This work has demonstrated that a detailed evaluation of ligand effects is feasible and can support the interpretation of experimental data, allowing some pathways to be ruled out with certainty. In addition, the energetic balance of competing reaction pathways has been shown to be quite subtle, illustrating and illuminating experimentally observed sensitivity to both ligand and substrate effects. Finally, this work has highlighted that multiple competing mechanisms may need to be considered for a full evaluation of ligand effects, and that both Gibbs energy and dispersion corrections are necessary to achieve reasonable agreement with available experimental data.

‡‡With the exception of the PhCl/PCy_3 system, where the calculated barrier for monoligated oxidative addition (path A) matches experimental data well, but calculations suggest that the bisligated oxidative addition of path C provides an alternative route with lower barriers.

Computational details

Structures were fully optimized in Gaussian (G03, see ESI for full citation†) with the standard B3LYP density functional[63] and a flexible double-ξ (triple-ξ with ECP on Pd and Br) polarized basis set, denoted as BS1 (full details are given in the ESI†). B3LYP/BS1 harmonic frequencies were used to identify stationary points and compute zero-point energy, enthalpic and entropic corrections. A polarizable continuum model was used to obtain single point solvation free energies with toluene solvent. Single point energy calculations were also carried out with a larger (augmented triple-ξ) basis set, again with ECP on Pd and Br (denoted as BS2), and with the B3LYP-D2 functional[64] as implemented in ORCA.[65] Full details of the computational methodology used, as well as further details about transition state scans and conformational searches, are given in the ESI.†

Acknowledgements

We thank Prof. Guy Orpen for helpful discussion of this work. NF thanks the EPSRC for the award of an Advanced Research Fellowships (EP/E059376/1), JNH holds a Royal Society Wolfson Research Merit Award and CLM thanks the CCDC, EPSRC and the School of Chemistry for funding, and CASCaM for the use of some computing facilities at the University of North Texas (CRIF, CHE-0741936).

Notes and references

1 (*a*) J. F. Hartwig, *Nature*, 2008, **455**, 314–322; (*b*) S. L. Buchwald, *Acc. Chem. Res.*, 2008, **41**, 1439; (*c*) C. A. Fleckenstein and H. Plenio, *Chem. Soc. Rev.*, 2010, **39**, 694–711; (*d*) C. Torborg and M. Beller, *Adv. Synth. Catal.*, 2009, **351**, 3027–3043; (*e*) C. C. C. Johansson Seechurn, M. O. Kitching, T. J. Colacot and V. Snieckus, *Angew. Chem., Int. Ed.*, 2012, **51**, 5062–5085.
2 R. F. Heck, *Nobel Lect.*, http://www.nobelprize.org/nobel_prizes/chemistry/laureates/2010/heck-lecture.html, 2010.
3 E.-i. Negishi, *Angew. Chem., Int. Ed.*, 2011, **50**, 6738–6764.
4 A. Suzuki, *Angew. Chem., Int. Ed.*, 2011, **50**, 6722–6737.
5 M. Kumada, *Pure Appl. Chem.*, 1980, **52**, 669.
6 J. K. Stille, *Angew. Chem., Int. Ed. Engl.*, 1986, **25**, 508.
7 Y. Hatanaka and T. Hiyama, *J. Org. Chem.*, 1988, **53**, 918.
8 A. R. Muci and S. L. Buchwald, *Top. Curr. Chem.*, 2002, **219**, 131.
9 J. F. Hartwig, *Acc. Chem. Res.*, 1998, **31**, 852.

10 (*a*) K. C. Lam, T. B. Marder and Z. Y. Lin, *Organometallics*, 2007, **26**, 758–760; (*b*) M. García-Melchor, A. A. C. Braga, A. Lledós, G. Ujaque and F. Maseras, *Acc. Chem. Res.*, 2013, **46**, 2626–2634.
11 K. J. Bonney and F. Schoenebeck, *Chem. Soc. Rev.*, 2014, DOI: 10.1039/C4CS00061G.
12 (*a*) L. Ackermann, R. Vicente and A. R. Kapdi, *Angew. Chem., Int. Ed.*, 2009, **48**, 9792–9826; (*b*) D. Balcells, E. Clot and O. Eisenstein, *Chem. Rev.*, 2010, **110**, 749–823; (*c*) X. Chen, K. M. Engle, D.-H. Wang and J.-Q. Yu, *Angew. Chem., Int. Ed.*, 2009, **48**, 5094–5115; (*d*) T. W. Lyons and M. S. Sanford, *Chem. Rev.*, 2010, **110**, 1147–1169.
13 (*a*) F. Barrios-Landeros, B. P. Carrow and J. F. Hartwig, *J. Am. Chem. Soc.*, 2009, **131**, 8141–8154; (*b*) J. C. Green, B. J. Herbert and R. Lonsdale, *J. Organomet. Chem.*, 2005, **690**, 6054–6067; (*c*) S. Shekhar and J. F. Hartwig, *Organometallics*, 2007, **26**, 340–351.
14 J. F. Hartwig, *Pure Appl. Chem.*, 1999, **71**, 1417–1423.
15 J. P. Stambuli, C. D. Incarvito, M. Bühl and J. F. Hartwig, *J. Am. Chem. Soc.*, 2004, **126**, 1184–1194.
16 S. Kozuch and J. M. L. Martin, *ACS Catal.*, 2011, **1**, 246–253.
17 J.-P. Corbet and G. Mignani, *Chem. Rev.*, 2006, **106**, 2651–2710.
18 A. F. Littke and G. C. Fu, *Angew. Chem., Int. Ed.*, 1998, **37**, 3387.
19 (*a*) F. Paul, J. Patt and J. F. Hartwig, *J. Am. Chem. Soc.*, 1994, **116**, 5969–5970; (*b*) F. Paul, J. Patt and J. F. Hartwig, *Organometallics*, 1995, **14**, 3030–3039; (*c*) J. Louie and J. F. Hartwig, *Tetrahedron Lett.*, 1995, **36**, 3609–3612.
20 J. F. Hartwig, *Acc. Chem. Res.*, 2008, **41**, 1534–1544.
21 (*a*) R. Martin and S. L. Buchwald, *Acc. Chem. Res.*, 2008, **41**, 1461–1473; (*b*) E. R. Strieter, D. G. Blackmond and S. L. Buchwald, *J. Am. Chem. Soc.*, 2003, **125**, 13978–13980; (*c*) D. S. Surry and S. L. Buchwald, *Angew. Chem., Int. Ed.*, 2008, **47**, 6338–6361.
22 (*a*) N. Fey, M. F. Haddow, J. N. Harvey, C. L. McMullin and A. G. Orpen, *Dalton Trans.*, 2009, 8183–8196; (*b*) J. Jover, N. Fey, J. N. Harvey, G. C. Lloyd-Jones, A. G. Orpen, G. J. J. Owen-Smith, P. Murray, D. R. J. Hose, R. Osborne and M. Purdie, *Organometallics*, 2010, **29**, 6245–6258; (*c*) J. Jover, N. Fey, J. N. Harvey, G. C. Lloyd-Jones, A. G. Orpen, G. J. J. Owen-Smith, P. Murray, D. R. J. Hose, R. Osborne and M. Purdie, *Organometallics*, 2012, **31**, 5302–5306.
23 G. J. J. Owen-Smith, J. Jover, N. Fey, J. N. Harvey, D. R. J. Hose, G. C. Lloyd-Jones, P. Murray, A. G. Orpen, R. Osborne and M. Purdie, in preparation for publication.
24 (*a*) J. Jover, N. Fey, M. Purdie, G. C. Lloyd-Jones and J. N. Harvey, *J. Mol. Catal. A: Chem.*, 2010, **324**, 39–47; (*b*) N. Fey, A. G. Orpen and J. N. Harvey, *Coord. Chem. Rev.*, 2009, **253**, 704–722.
25 (*a*) C. L. McMullin, B. Rühle, M. Besora, A. G. Orpen, J. N. Harvey and N. Fey, *J. Mol. Catal. A: Chem.*, 2010, **324**, 39–47; (*b*) C. L. McMullin, J. Jover, J. N. Harvey and N. Fey, *Dalton Trans.*, 2010, **39**, 10833–10836.
26 (*a*) C. J. Cramer and D. G. Truhlar, *Acc. Chem. Res.*, 2008, **41**, 760–768; (*b*) J. N. Harvey, *Faraday Discuss.*, 2010, **145**, 487–505.
27 N. Fey, B. M. Ridgway, J. Jover, C. L. McMullin and J. N. Harvey, *Dalton Trans.*, 2011, **40**, 11184–11191.
28 R. F. Ribeiro, A. V. Marenich, C. J. Cramer and D. G. Truhlar, *J. Phys. Chem. B*, 2011, **115**, 14556–14562.
29 (*a*) G. C. Fu, *Acc. Chem. Res.*, 2008, **41**, 1555–1564; (*b*) F. Schoenebeck and K. N. Houk, *J. Am. Chem. Soc.*, 2010, **132**, 2496–2497.
30 (*a*) E. A. Mitchell and M. C. Baird, *Organometallics*, 2007, **26**, 5230–5238; (*b*) E. A. Mitchell, P. G. Jessop and M. C. Baird, *Organometallics*, 2009, **28**, 6732–6738; (*c*) A. Kurbangalieva, D. Carmichael, K. K. M. Hii, A. Jutand and J. M. Brown, *Chem. – Eur. J.*, 2014, **20**, 1116–1125.
31 (*a*) P. Vidossich, G. Ujaque and A. Lledos, *Chem. Commun.*, 2014, **50**, 661–663; (*b*) K. Vikse, T. Naka, J. S. McIndoe, M. Besora and F. Maseras, *ChemCatChem*, 2013, **5**, 3604–3609.
32 (*a*) E. Lyngvi and F. Schoenebeck, *Tetrahedron*, 2013, **69**, 5715–5718; (*b*) F. Proutiere and F. Schoenebeck, *Angew. Chem., Int. Ed.*, 2011, **50**, 8192–8195.
33 (*a*) Z. Li, Y. Fu, Q.-X. Guo and L. Liu, *Organometallics*, 2008, **27**, 4043–4049; (*b*) H. M. Senn and T. Ziegler, *Organometallics*, 2004, **23**, 2980–2988; (*c*) L. M. Alcazar-Roman, J. F. Hartwig, A. L. Rheingold, L. M. Liable-Sands and I. A. Guzei, *J. Am. Chem. Soc.*, 2000, **122**, 4618–4630; (*d*) M. Ahlquist, P. Fristrup, D. Tanner and P.-O. Norrby, *Organometallics*, 2006, **25**, 2066–2073.
34 (*a*) C. Amatore and F. Pfluger, *Organometallics*, 1990, **9**, 2276–2282; (*b*) V. G. Andrianov, I. S. Akhrem, N. M. Chistovalova and Y. T. Struchkov, *Zh. Strukt. Khim.*, 1976, **17**, 135.
35 M. S. G. Ahlquist and P.-O. Norrby, *Angew. Chem., Int. Ed.*, 2011, **50**, 11794–11797.
36 J.-F. Fauvarque, F. Pflüger and M. Troupel, *J. Organomet. Chem.*, 1981, **208**, 419–427.
37 J. P. Stambuli, M. Bühl and J. F. Hartwig, *J. Am. Chem. Soc.*, 2002, **124**, 9346.
38 (*a*) T. Aoki, Y. Ishii, Y. Mizobe and M. Hidai, *Chem. Lett.*, 1991, **20**, 615–618; (*b*) J. P. Flemming, M. C. Pilon, O. Y. Borbulevitch, M. Y. Antipin and V. V. Grushin, *Inorg. Chim. Acta*, 1998, **280**, 87–98.
39 A. G. Sergeev, A. Zapf, A. Spannenberg and M. Beller, *Organometallics*, 2008, **27**, 297–300.
40 S. Moncho, G. Ujaque, A. Lledos and P. Espinet, *Chem. – Eur. J.*, 2008, **14**, 8986–8994.
41 J. Tomasi, B. Mennucci and R. Cammi, *Chem. Rev.*, 2005, **105**, 2999–3094.
42 (*a*) A. A. C. Braga, G. Ujaque and F. Maseras, *Organometallics*, 2006, **25**, 3647–3658; (*b*) H. Jacobsen and L. Cavallo, *ChemPhysChem*, 2012, **13**, 562–569.
43 (*a*) M. Besora, A. A. C. Braga, G. Ujaque, F. Maseras and A. Lledos, *Theor. Chem. Acc.*, 2010, 639–646; (*b*) F. Ragone, A. Poater and L. Cavallo, *J. Am. Chem. Soc.*, 2010, **132**, 4249–4258.

44 (*a*) C. Amatore and A. Jutand, *Acc. Chem. Res.*, 2000, **33**, 314–321; (*b*) C. Amatore, G. Le Duc and A. Jutand, *Chem. – Eur. J.*, 2013, **19**, 10082–10093; (*c*) L. J. Goossen, D. Koley, H. L. Hermann and W. Thiel, *Organometallics*, 2006, **25**, 54–67.
45 F. H. Allen, *Acta Crystallogr., Sect. B: Struct. Sci.*, 2002, **58**, 380.
46 M. Ahlquist and P.-O. Norrby, *Organometallics*, 2007, **26**, 550–553.
47 N. Fey, A. C. Tsipis, S. E. Harris, J. N. Harvey, A. G. Orpen and R. A. Mansson, *Chem. – Eur. J.*, 2006, **12**, 291–302.
48 N. Miyaura and A. Suzuki, *Chem. Rev.*, 1995, **95**, 2457–2483.
49 A. Ariafard and B. F. Yates, *J. Am. Chem. Soc.*, 2009, **131**, 13981–13991.
50 B. E. Mann and A. Musco, *J. Chem. Soc., Dalton Trans.*, 1975, 1673–1677.
51 Y. Minenkov, A. Singstad, G. Occhipinti and V. R. Jensen, *Dalton Trans.*, 2012, **41**, 5526–5541.
52 A. Jutand and A. Mosleh, *Organometallics*, 1995, **14**, 1810–1817.
53 (*a*) D. W. Old, J. P. Wolfe and S. L. Buchwald, *J. Am. Chem. Soc.*, 1998, **120**, 9722; (*b*) J. P. Wolfe, S. Wagaw, J.-F. Marcoux and S. L. Buchwald, *Acc. Chem. Res.*, 1998, **31**, 805–818; (*c*) J. P. Wolfe, H. Tomori, J. P. Sadighi, J. Yin and S. L. Buchwald, *J. Org. Chem.*, 2000, **65**, 1158.
54 T. E. Barder, S. D. Walker, J. R. Martinelli and S. L. Buchwald, *J. Am. Chem. Soc.*, 2005, **127**, 4685–4696.
55 S. D. Walker, T. E. Barder, J. R. Martinelli and S. L. Buchwald, *Angew. Chem., Int. Ed.*, 2004, **43**, 1871–1876.
56 (*a*) T. E. Barder, M. R. Biscoe and S. L. Buchwald, *Organometallics*, 2007, **26**, 2183–2192; (*b*) T. E. Barder and S. L. Buchwald, *J. Am. Chem. Soc.*, 2007, **129**, 12003–12010; (*c*) S. Kozuch and J. M. L. Martin, *Chem. Commun.*, 2011, **47**, 4935–4937.
57 M. R. Biscoe, T. E. Barder and S. L. Buchwald, *Angew. Chem., Int. Ed.*, 2007, **46**, 7232.
58 F. Barrios-Landeros, B. P. Carrow and J. F. Hartwig, *J. Am. Chem. Soc.*, 2008, **130**, 5842–5843.
59 W.-J. Sun, W. Chu, L.-J. Yu and C.-F. Jiang, *Chin. J. Chem. Phys.*, 2010, **23**, 175–179.
60 M. Tanaka, *Acta Crystallogr., Sect. C: Cryst. Struct. Commun.*, 1992, **48**, 739–740.
61 (*a*) J. Vignolle, H. Gornitzka, B. Donnadieu, D. Bourissou and G. Bertrand, *Angew. Chem., Int. Ed.*, 2008, 47; (*b*) D. V. Partyka, T. J. Robilotto, M. Zeller, A. D. Hunter and T. G. Gray, *Organometallics*, 2008, **27**, 28–32.
62 B. Schlummer and U. Scholz, *Adv. Synth. Catal.*, 2004, **346**, 1599–1626.
63 (*a*) A. D. Becke, *Phys. Rev. A*, 1988, **38**, 3098–3100; (*b*) A. D. Becke, *J. Chem. Phys.*, 1993, **98**, 5648–5652; (*c*) C. T. Lee, W. T. Yang and R. G. Parr, *Phys. Rev. B: Condens. Matter*, 1988, **37**, 785–789; (*d*) S. H. Vosko, L. Wilk and M. Nusair, *Can. J. Phys.*, 1980, **58**, 1200–1211; (*e*) B. Miehlich, A. Savin, H. Stoll and H. Preuss, *Chem. Phys. Lett.*, 1989, **157**, 200–206; (*f*) J. C. Slater, *Quantum Theory of Molecules and Solids, Vol. 4: The Self-Consistent Field for Molecules and Solids*, McGraw-Hill, New York, 1974.
64 S. Grimme, *J. Comput. Chem.*, 2006, **27**, 1787–1799.
65 ORCA, *An Ab Initio, DFT, and Semiempirical Electronic Structure Package Version 2.6.35*, F. Neese, Universität Bonn, Germany, 2007.
66 C. A. Tolman, *Chem. Rev.*, 1977, **77**, 313–348.